Environmental Science & Technology

pubs.acs.org/est

Article

Uptake of Hydrogen Peroxide from the Gas Phase to Grain Boundaries: A Source in Snow and Ice

Angela C. Hong, Thomas Ulrich, Erik S. Thomson, Jürg Trachsel, Fabienne Riche, Jennifer G. Murphy, D. James Donaldson, Martin Schneebeli, Markus Ammann, and Thorsten Bartels-Rausch*

Cite This: *Environ. Sci. Technol.* 2023, 57, 11626–11633

Read Online

ACCESS | Metrics & More | Article Recommendations | Supporting Information

ABSTRACT: Hydrogen peroxide is a primary atmospheric oxidant significant in terminating gas-phase chemistry and sulfate formation in the condensed phase. Laboratory experiments have shown an unexpected oxidation acceleration by hydrogen peroxide in grain boundaries. While grain boundaries are frequent in natural snow and ice and are known to host impurities, it remains unclear how and to which extent hydrogen peroxide enters this reservoir. We present the first experimental evidence for the diffusive uptake of hydrogen peroxide into grain boundaries directly from the gas phase. We have machined a novel flow reactor system featuring a drilled ice flow tube that allows us to discern the effect of the ice grain boundary content on the uptake. Further, adsorption to the ice surface for temperatures from 235 to 258 K was quantified. Disentangling the contribution of these two uptake processes shows that the transfer of hydrogen peroxide from the atmosphere to snow at temperatures relevant to polar environments is considerably more pronounced than previously thought. Further, diffusive uptake to grain boundaries appears to be a novel mechanism for non-acidic trace gases to fill the highly reactive impurity reservoirs in snow's grain boundaries.

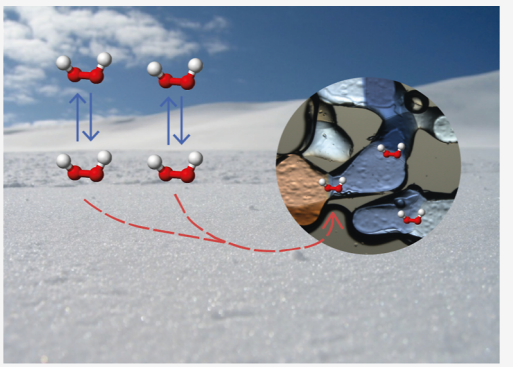

KEYWORDS: *Arctic, snow, oxidation, chromophore, H_2O_2, HOOH, atmospheric oxidant*

INTRODUCTION

Hydrogen peroxide (H_2O_2) is a central inorganic oxidant in the hydrosphere and the atmosphere.[1] In snow, it acts as a chromophore and a precursor for HO_x.[2−5] Temperature-dependent uptake and emission of H_2O_2 from snow alter gas-phase concentrations on daily timescales.[6,7] Recent interest in the multiphase phase chemistry of H_2O_2 was sparked by a report on the autonomous formation of H_2O_2 at the interface of micron-sized droplets.[8,9] In ice and snow, grain boundaries and their junctions provide micron-sized confined environments hosting impurities and multiphase reactions.[10−14] In particular, oxidation reactions such as that of H_2O_2 with benzoic acid are highly accelerated in these locations in ice.[15] We, therefore, investigate whether the uptake of H_2O_2 from the gas phase is a source of H_2O_2 in grain boundaries of snow. Its presence there might help better assess the environmental impact of the previous findings on accelerated reactivity.

An environmental source of chemical impurities in ice clouds, snowflakes, or snowpacks on the ground is the scavenging of trace gases.[14] Adsorption at the surface routes in forming hydrogen bonds at the interface and is fundamentally identical for snow and ice. At environmental trace gas concentrations, it quickly leads to an equilibrium surface coverage of the adsorbate as a function of temperature and partial pressure.[16,17] Previous work has characterized this adsorption equilibrium for H_2O_2 at temperatures up to 223 K with relevance as a loss process of this atmospheric oxidant to ice clouds in the upper troposphere.[18,19] In this work, we quantify the adsorption of H_2O_2 to ice for higher temperatures that are most relevant for polar and alpine environments where snow is present, such as during Arctic spring, a period with significant active photochemistry in snow.

Adsorbates may also diffuse along grain boundaries of ice and snow.[14] For acidic trace gases, such as HNO_3,[20,21] HCl,[21,22] HONO,[23] and SO_2,[24] this loss process was proposed to explain an uptake acting on longer time scales than adsorption,[25] but direct evidence is missing. Interestingly, weaker organic acids, such as acetic and formic acid, adsorb to the air−ice interface without diffusing into grain boundaries.[26] X-ray excited electron spectroscopy work revealed that strong acids such as HNO_3 and HCl interact with the air−ice interface forming liquid-like regions, while formic acid and acetic acid do not.[27−31] H_2O_2 was chosen because it has a high solubility in water, and this work provides clear experimental

Received: February 22, 2023
Revised: July 9, 2023
Accepted: July 10, 2023
Published: July 27, 2023

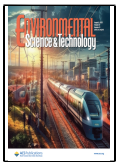

evidence of enhancing the overall uptake of H_2O_2 to snow by diffusion into the grain boundaries despite its low acidity.

To discern the effect of the ice microstructure on the uptake of H_2O_2, we have machined a novel flow reactor system featuring a drilled ice flow tube (DIFT). We use two distinct ice morphologies for the DIFT: monocrystalline (MC) ice, which is characterized by large crystals domains with a reduced grain boundary network, and polycrystalline (PC) ice, which has relatively more and smaller crystal domains and a more extensive grain boundary network within a comparable volume.

MATERIALS AND METHODS

The experiment consists of an H_2O_2 source to provide a steady gas-phase concentration of H_2O_2 in humidified N_2 carrier gas, a flow tube where the H_2O_2 is passed over an ice sample that can be by-passed, and an H_2O_2 detector to monitor changes to the gas-phase H_2O_2 concentration in the carrier gas downstream of the flow tube. The flow tube was a DIFT, where a hole is bored through an ice block or an ice-coated-wall flow tube. A schematic of the experimental setup is shown in the Supporting Information (Figure S1).

Preparing Drilled Ice Flow Tubes. The ice block characterized by large crystal domains (MC) has been purchased from the ICE Factory of Switzerland (www.icefactory.ch). The purchased ice block is not treated before use. Polycrystalline ice (PC) is grown by freezing ultraclean water (Millipore Milli-Q, 0.05 μS) at 253 K. From each MC and PC sample, one drilled ice flow tube (DIFT) is made by cutting the respective ice into blocks of 10 cm lengths and drilling a 6 mm borehole longitudinally through the middle of each block. At each end, the boreholes were widened to approximately 9 mm to attach fittings by screwing in preheated threads (Bola, Germany), which temporarily melts the ice and, upon refreezing, creates gas-tight connections. The connections also leave the inner borehole diameter flush with the inner fitting diameter to allow for smooth flow transitions. Additional water is frozen around the fitting external to the connector to increase durability. The DIFT boreholes are 80 mm long. Four experiments were done with one DIFT tube each on 2 days. Experiments started with the lowest H_2O_2 concentration, which then increased from experiment to experiment. DIFT tubes were sealed and stored at −20 °C overnight. Before the first experiment each day, the tubes were purged with humidified carrier gas for 30 min. Between experiments on the same day, desorption experiments served to purge the tubes (see Results and Discussion).

Imaging Drilled Ice Flow Tubes. Thin DIFT cross-sections (250 μm) are prepared after drilling and imaged using a compound optical microscope with a nadir polarized light source as described earlier.[32,33]

Coated Wall Flow Tube. Coated wall flow tube experiments are done in quartz glass tubes with 8 mm inner diameters. The inner surface of the quartz tube is covered with ice.[34] Briefly, the quartz tube is internally etched with a solution of 5% hydrofluoric acid in water and subsequently is rinsed several times with purified water (Millipore Milli-Q, 0.05 μS). After rinsing, 8−10 mL of ultra-pure water (for high-performance liquid chromatography use, Fluka 14263) or laboratory Milli-Q water (Millipore Milli-Q, 0.05 μS) are pipetted into the quartz tube. Excess water is removed by orienting the quartz tube vertically for 1 min and draining. An ice film is formed at 258 K by slowly rotating the coated flow tube in a snuggly fitted double-mantled cooling jacket. This procedure results in thin ice films with an average thickness of 10 μm, as determined by mass. Quartz tubes of either 80 or 45 cm in length are used in this work. Data obtained with ice made from ultra-pure and Milli-Q water are in excellent agreement. For each experiment, a new coating was prepared.

H_2O_2 Source. For the DIFT experiments, H_2O_2 is introduced to the experiment by adding a small stream of N_2 carrier gas over a frozen solution of 30% H_2O_2 (Perhydrol p.a., 7209 Merck) at 248 K. For coated wall flow tube experiments, gas-phase H_2O_2 is dosed from a custom-built permeation tube. For this, a liquid solution of 30% H_2O_2 (Perhydrol p.a., 7209 Merck) fills a 17.4 cm long, thin-walled fluorinated ethylene propylene (FEP) tube sealed at both ends. The permeation tube is placed in a commercial permeation oven (VICI Dynacalibrator) at 323 K. A flow of pure nitrogen (Carbagas 99.9995% purity) through the permeation oven transports the gas phase H_2O_2 into the experimental setup.

Detection of H_2O_2. Gas-phase H_2O_2 is measured using a commercial H_2O_2 analyzer with a detection limit of 100 ppt, corresponding to 2.5×10^9 molecules per cm^3 at 298 K and 1 atm (Aero-Laser, Germany, AL2021). The instrument relies on a fluorometric method, by which H_2O_2 is stripped from the gas phase in a glass coil and subsequently reacts with *p*-hydroxyphenyl acetic acid and peroxidase forming a fluorescence dimer. This method detects all peroxides in the solution. The reagents used for the analyzer were: Potassium phthalate (monobasic, 96148 Fluka), EDTA (Titriplex III p.a., 1.08418 Merck), NaOH (1 N, 71463 Fluka), formaldehyde (37 wt % in water, 252549 Sigma-Aldrich), *p*-hydroxyphenyl acetic acid (98%, H5,000-4 Sigma-Aldrich), and peroxidase (from horseradish, P8250 Sigma-Aldrich). The reagents are dissolved in double distilled water (3478.2 Roth). The instrument is calibrated with diluted liquid solutions of H_2O_2 (Perhydrol 30% p.a., 7209 Merck), which are titrated against a permanganate solution (permanganate 1/500 mol 38136 Fixanal) of certified concentration.

Flow System. The tubing of the flow system consisted of perfluoro-alkoxy copolymer (PFA). The flow through the coated wall flow tube is controlled by the H_2O_2 analyzer and set to either 2000 mL min^{-1} STP (standard temperature and pressure: 273.15 K and 1 bar) or 500 mL min^{-1} STP, respectively. The flow through the permeation source is constant at 1500 mL min^{-1} STP. For the drilled flow tube experiments, the flow via the H_2O_2 source is set to 20 mL min^{-1} and mixed with a humidified flow of 215−230 mL min^{-1} N_2. After passing the drilled flow tube or by-pass, the gas flow was diluted with 1900−2000 mL min^{-1} to quickly transport the H_2O_2 to the analyzer operated with a flow of 1500 mL min^{-1}.

RESULTS AND DISCUSSION

Characterizing Grain Boundaries. Figure 1 shows microscopy images of MC- and PC-DIFT thin cross-sections imaged using cross-polarized light. Due to the birefringent nature of ice, different crystal orientations are visualized as distinct color regions when viewed with polarized light.[33,35] The PC-DIFT sample (Figure 1B) shows nine distinct grain areas of different colors. The MC-DIFT image (Figure 1A) displays much more homogeneity, i.e., a single ice crystal surrounding the borehole in this section. The figure confirms that the PC-DIFT sample contains relatively more single crystals and, thus, a more extensive grain boundary network reaching the air−ice interface than the MC-DIFT sample for

https://doi.org/10.1021/acs.est.3c01457
Environ. Sci. Technol. 2023, 57, 11626−11633

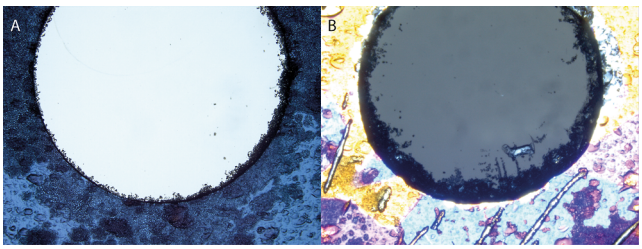

Figure 1. Thin cross-sections as obtained by polarization microscopy of MC ice (A) and the increased polycrystallinity of PC ice (B). The imaged boreholes have a 6 mm inner diameter. Individual crystals appear as uniformly colored grains. The images further show granular, dark-shaded features in large fractions of the image that appear to originate from debris associated with the microtome-cutting procedure. These were not visually detectable following the uptake-desorption experiments.

the same cross-sectional area. The image in Figure 1B shows 6 grain boundaries at the flow tube's air−ice interface of 6 mm diameter (or 19 mm length). The corresponding 0.3 grain boundaries per mm lie within the range for natural snow. Synchrotron-based diffraction-contrast tomography images indicate 0.5−2 grain boundaries per mm for hardened, aged snow.[36,37] Freshly fallen surface snow is less dense and can be expected to have fewer grain boundaries, but to our knowledge, data are unavailable. In the following, we describe the fate of H_2O_2 upon adsorption to these ice samples with different grain-boundary densities.

Uptake to Grain Boundaries and the Surface. The upper panels in Figure 2 display uptake curves, that is, the change in the gas-phase H_2O_2 number density in the carrier gas evolving upon contact with the ice for the MC-DIFT (Figure 2A) and PC-DIFT (Figure 2B) experiments. The ice is exposed to between 1.4×10^{12} and 2.8×10^{12} molecules H_2O_2 cm^{-3} in the carrier gas. The flow tubes were bypassed at $t < 0$ min, and the humidified carrier gas with H_2O_2 was fed directly to the analyzer. At $t = 0$ min, the gas flow was redirected through the flow tubes, and the uptake curves reveal a fast loss of gas phase H_2O_2. The uptake curves slowly recover towards the initial gas-phase H_2O_2 concentration until the gas flow is directed again via the bypass at $t = 60$ min. Focusing on the recovery level reached toward the end of the experiment's time scale reveals that the ongoing net uptake of H_2O_2 in the PC-DIFT is clearly more pronounced than in the MC-DIFT. This difference in the uptake behavior of H_2O_2 for the PC-DIFT compared to the MC-DIFT is attributed to a more extensive network of grain boundaries at the air−ice interface (Figure 1). The diffusion into such reservoirs has been proposed as a candidate to explain the slow, long-term recovery of uptake curves.[25] This work links the direct observation of grain boundary content in ice samples with the diffusive loss. We want to stress the environmental relevance of this direct experimental evidence for H_2O_2 uptake from the gas phase to the grain boundaries, where H_2O_2 is a potent oxidant.[15] It is important to note that the relevance of diffusive uptake varies not only with grain boundary content but also from species to species. Bartels-Rausch et al.[26] showed that for the non-acidic volatile organics acetone and methanol, diffusion into grain boundaries is not a vital loss process in snow. The direct and long-term uptake of H_2O_2 from the gas phase is the first evidence of a non-acidic trace gas entering grain boundaries, casting questions on the importance of acidity as a driving factor.

Reversibility of Uptake. We further explore the impact of grain boundaries on the reversibility of H_2O_2 uptake to MC- versus PC-DIFT. The lower panels in Figure 2 show

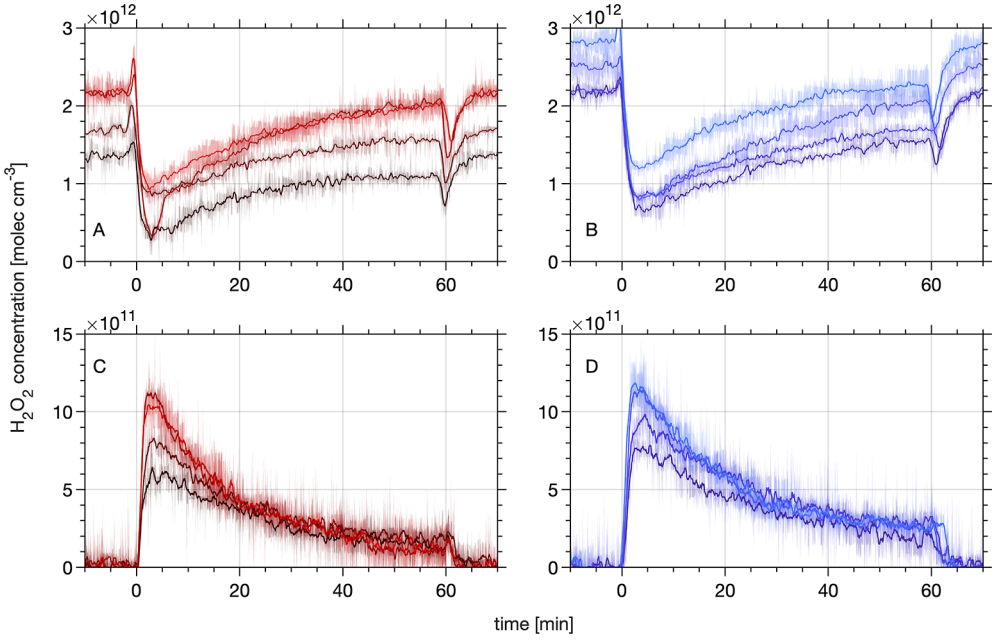

Figure 2. H_2O_2 uptake to and release from MC-DIFT (solid red lines) and PC-DIFT (solid blue lines) as a function of time at 253 K. Before $t = 0$ min and after $t = 60$ min, the gas flow is directed through the bypass. Panels (A,B) show the loss of H_2O_2 to the ice from the carrier gas during uptake experiments. The short dip in signal intensity at $t = 60$ min is attributed to H_2O_2 adsorbing at the walls of the dosing line. Panels (C,D) show the time traces of subsequent H_2O_2 desorption from the ice to the carrier gas. Colors denote the 4 repetitions for each MC- and PC-DIFT, respectively. The color density indicates the order of the repetitions at varying concentrations, with the darkest lines showing the first run. Each line shows the average of two measurements, and the shaded areas represent the standard error and, thus, indicate the uncertainty of data processing.

https://doi.org/10.1021/acs.est.3c01457
Environ. Sci. Technol. 2023, 57, 11626−11633

desorption curves, where humidified carrier gas without added H_2O_2 was passed via the DIFTs that had previously been exposed to H_2O_2 (upper panel). The desorption curves probe the release of H_2O_2 from the ice samples. They show similar shapes with rapid increases of the gas-phase H_2O_2 concentration when the carrier gas flow through the DIFTs is initiated at t = 0 min. A slow decaying release follows for both the MC-DIFT and the PC-DIFT. The shape similarity between such uptake and desorption curves has previously been noted.[38] Generally, the magnitude of H_2O_2 release observed during the desorption experiments scales with the gas-phase concentration of H_2O_2 that the DIFTs were exposed to during the uptake experiments. The highest release of H_2O_2 to the gas phase of 3.0×10^{11} molecule s^{-1} cm^{-2} (light red) and 3.3×10^{11} molecule s^{-1} cm^{-2} (light blue), yielded gas-phase maximum concentrations of 11×10^{11} molecule cm^{-3} (light red) and 12×10^{11} molecule cm^{-3} (light blue) in the desorption experiments for the MC- and PC-DIFT, respectively. These were observed in runs that followed uptake experiments with the highest gas-phase concentrations (light red and light blue in the upper panels of Figure 2). For both samples, the release of H_2O_2 is not complete after 60 min, indicating that the release occurs at a slower apparent rate than the uptake. The median recovery is 69% for experiments with MC-DIFT, significantly different from about 56% recovery determined for the PC-DIFT (see Supporting Information, Figure S3). A qualitative explanation for the longer residence time during the recovery experiments might be that in this mode, the concentration gradient drives diffusion back toward the air−ice interface, where the carrier gas passes the ice, and deeper into the ice. During the uptake experiments, the concentration gradients drive the net diffusion of H_2O_2 exclusively from the air−ice into the bulk ice interior. From the surface, H_2O_2 readily desorbs and is carried away by the gas stream once the desorption experiment begins. This leads to changes to the concentration gradients that drive bulk diffusion and a diffusive flux in the reverse direction toward the carrier-gas−ice interface establishes. However, because the H_2O_2 concentrations remain low in the interior of the DIFT tube bulk ice, diffusion away from the air−ice interface also continues. The partial irreversibility on the time scales of the uptake agrees with Conklin et al.,[38] who found between 33 and 47% recovery. That their recovery is lower than that found in our PC-DIFT experiments might be due to a different grain boundary density in their samples and their longer experimental time scales that would allow for more extensive diffusion. Also, differences in pressure and flow tube geometry between individual flow tube studies, where the transport and retention of trace gases involve multiple re-adsorption steps, might hamper direct comparison. Nevertheless, Conklin et al.[38] used sintered ice spheres that likely provide a significant but unknown grain boundary density.[33] Interestingly, a different behavior was observed for the acidic HCl. McNeill et al.[39] concluded that HCl is reversibly adsorbed to grain boundaries and observed full recovery within experimental time scales of up to 50 min at −60 °C.

Quantifying the Diffusive-like Uptake. Our observation that grain boundaries in polycrystalline ice provide a sink for gas-phase H_2O_2 motivates quantification by comparing the observed uptake curves with theoretical predictions. Such comparisons have been used to identify the uptake mechanism at a wide range of experimental settings and time scales, tremendously impacting the shape of uptake curves.[25] In Figure 3, we compare the experimental uptake curves to a kinetic model with coupled adsorption and diffusive uptake.

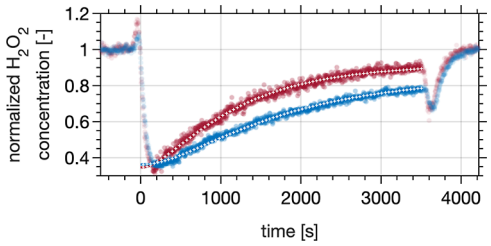

Figure 3. Uptake curves for MC-DIFT (red circles) and PC-DIFT (blue circles). The DIFTS were exposed to the H_2O_2 in the carrier gas at t = 0. The results from 4 individual experiments were normalized to the H_2O_2 gas-phase concentration before t = 0 and averaged. Filled circles denote the data that were fitted (white lines).

Equation 1 gives the time-dependent H_2O_2 number density exiting the DIFT ($n_{DIFT}(t)$) normalized to the initial concentration (n_0) for the coupled adsorption-diffusion model as detailed in the Supporting Information (Supporting Information, "The resistor model").[40−42] Here, the length of the DIFT is denoted by x, the surface area of the DIFT borehole by A, the volume of DIFT borehole is V, $\bar{\nu}$ is the mean thermal velocity of the gas molecules, u is the linear gas velocity, and t the time. The mass accommodation coefficient α_c describes the fraction of molecules entering the condensed phase relative to those colliding with the interface. The time constant of Langmuir adsorption is denoted by λ. The free parameter we determine by fitting in this work is the product $H\sqrt{D}$, where H is the dimensionless Henry's solubility law constant and D is the H_2O_2 diffusion constant in the solid phase. The solubility H is defined as the ratio between condensed-phase concentration and gas-phase concentration of a species.[43]

$$\frac{n_{DIFT}(t)}{n_0} = \exp\left[-\frac{x}{u}\frac{A}{V}\frac{\bar{\nu}}{4}\left(\frac{1}{\frac{1}{\alpha_c(1-e^{-\lambda t})} + \frac{\bar{\nu}\sqrt{\pi t}}{4H\sqrt{D}}} + \alpha_c e^{-\lambda t}\right)\right] \quad (1)$$

Figure 3 presents the asymptotic fit to the last 500 s of the uptake curves and shows the excellent capture of the observations by the coupled kinetic model. The agreement confirms that the H_2O_2 air−ice interaction can be understood as a combination of adsorption to the surface and the diffusive loss from the surface acting on longer time scales. We derive 3 and 7 cm $s^{-1/2}$ for $H\sqrt{D}$ for the MC- and PC-DIFT uptake curves from the fitting. That the value of $H\sqrt{D}$ is larger for the PC-DIFT compared to the MC-DIFT by a factor of about two clearly shows the importance of grain boundaries for long-term, diffusive uptake of H_2O_2 into the ice matrix. In this analysis, the derived $H\sqrt{D}$ must be understood as a combination of a grain-boundary-related $H\sqrt{D}$ and the $H\sqrt{D}$ in crystalline ice. Taken that the solubility and the diffusivity of H_2O_2 in the ice crystal and the grain boundary are identical for both DIFT tubes, we assign the difference in the $H\sqrt{D}$ term to varying grain boundary numbers in both samples. This implies that both the loss rate of H_2O_2 and the apparent solubility are enhanced in environmental ice and snow as a function of grain boundary content. In the following, we estimate $H\sqrt{D}$ values for the diffusive loss of H_2O_2 into

https://doi.org/10.1021/acs.est.3c01457
Environ. Sci. Technol. 2023, 57, 11626−11633

single crystalline ice to support the hypothesis that this long-term loss process cannot explain the derived $H\sqrt{D}$ alone. Neither the solubility nor the diffusivity of H_2O_2 in single crystalline ice is known. Supposing H_2O_2 has a similar solubility and diffusivity in ice as HCl, $H\sqrt{D}$ of 0.2−2.8 cm $s^{-1/2}$ can be calculated at −25 °C based on published solubility and diffusivity data.[44] The scatter reflects experimental uncertainty. The similarity of the observed $H\sqrt{D}$ in MC-DIFT with this estimate indicates that diffusion into the crystalline ice phase could explain a significant fraction of the long-term trend observed in MC-DIFT experiments but not that in PC-DIFT. However, the solubility of HCl in ice is exceptionally high compared to HNO_3, another trace gas of atmospheric relevance. Solubilities in single crystalline ice (solid solution) of 0.1 mol/L for HCl versus 0.001 mol/L for HNO_3 have been found at partial pressures of 0.2×10^{-3} and 0.7×10^{-3} Pa and temperatures of −25 °C.[44,45] Just as H_2O_2, HNO_3 is highly soluble in water[43] and, therefore, we estimate the solubility of H_2O_2 in ice in the following based on HNO_3 solid solution data. For HNO_3, $H\sqrt{D}$ values of 0.008−0.02 can be derived, which are significantly smaller than the results even for MC-DIFT. If we assume that the solubility of H_2O_2 in crystalline ice is closer to HNO_3 than to HCl, the contribution of the solid-state diffusion to the long-term uptake in our experiments is negligible, and consequently, diffusion into grain boundaries would dominate the long-term uptake of H_2O_2 to ice in both samples.

The direct comparison of the uptake to samples that differ in grain-boundary density and that the diffusive loss is larger than expected for diffusion into the ice crystal strongly suggests that the observed long-term DIFT uptake is driven by diffusion into grain boundaries. The preference of H_2O_2 for grain boundaries in environmental snow and ice might result in significant variations in the local concentration of H_2O_2. This is relevant as such non-uniform chemical morphologies and highly concentrated patches of reactants at grain boundaries and elsewhere in the ice have recently been shown to impact chemical reactivity in frozen systems strongly.[13,15,46] Grain boundaries in natural snowpacks occur at the contact face of individual snow grains.[47] As grain size, shape, and arrangement change with time in snowpacks (metamorphism),[48] detailed studies observing the impact of grain boundaries at different stages of metamorphism are timely to elucidate the mechanism and the environmental impact more extensively.

Temperature Trend of Surface Adsorption. Given that the uptake curves are well described by a combination of long-term diffusion and short-term adsorption (eq 1, Figure 3), numerically integrating the initial part of the uptake curves further allows us to quantify the H_2O_2 partitioning equilibrium between the ice surface and the gas phase (Supporting Information, Figure S4). Figure 4 shows the temperature trend and the magnitude of the adsorption equilibrium at temperatures from 258 to 235 K derived in coated wall flow tube experiments and in the MC-DIFT and the PC-DIFT. The observed negative temperature trend of the partitioning coefficient is strong experimental proof for an adsorption process during this initial uptake regime that can be well described with a simple Langmuir model.[16,18] The partitioning coefficient, K_{LinC}, is defined as the surface concentration of the adsorbed H_2O_2 in molecules cm^{-2}, divided by the gas-phase concentration in molecules cm^{-3}. The ice−air interface has become more disordered in this temperature range.[14] The consistent negative temperature trend with extrapolated results

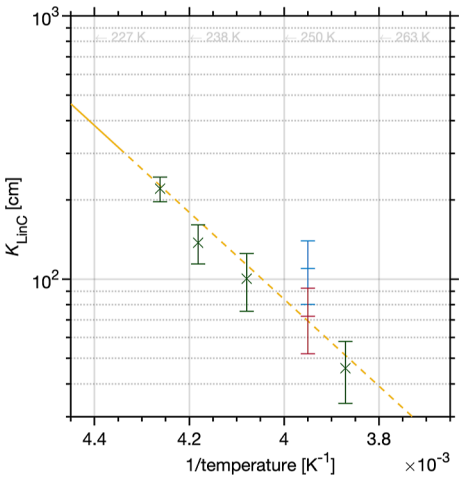

Figure 4. Linear Langmuir partitioning coefficient of H_2O_2 vs temperature, including data for the coated wall flow tube (green markers), MC-DIFT (red marker), and PC-DIFT (blue marker). Error bars represent one standard deviation from repeated experiments. Also shown is a parameterization of the partitioning coefficient based on published data[18] (solid yellow line) and its extrapolation to warmer temperatures (dashed yellow line).

from an earlier low-pressure coated wall flow tube study between 203 and 233 K[18] indicates that the presence of this disordered interface [also referred to as quasi-liquid-layer (QLL), pre-melting] does not change the uptake behavior of H_2O_2 up to 260 K.

The reported partitioning coefficients between 258 and 235 K make H_2O_2 one of the stickier atmospheric trace gases compared to volatile alcohols, aldehydes, and ketones. Its partitioning coefficient is 2−3 orders of magnitude larger than that of methanol or acetone with 10^0 and 10^{-1} cm, respectively, at 240 K and even larger than that of acetic acid for which a partitioning coefficient of 10^1 cm has been found at 240 K.[49] For comparison, strong acids such as HCl have partitioning coefficients of 10^4 cm at 240 K.[50] The reported partitioning implies that a large fraction of H_2O_2 is found adsorbed to surface snow and not in the gas phase in this temperature range typical for the Arctic. A surface area of 59 cm^2 per cm^3 has been reported for freshly fallen snow,[51] which yields 2×10^{12} molecules of H_2O_2 adsorbed per cm^3 of snow at 260 K and 7×10^{12} molecules per cm^3 at 240 K with the partitioning coefficients reported in this work; while the air above snow holds 10^9 molecules cm^{-3}. Because the air−ice interface of coated wall ice films is smooth on a molecular level,[16] and that of the DIFTs can be expected to be so because any initial surface roughness and microstructures are generally smoothed by sintering with time,[52] the adsorption process and the partitioning coefficients are invariant between ice and snow. Such gas-phase concentration of H_2O_2 used in this estimate is typical in the Arctic.[53] For technical reasons, experiments have been done with higher H_2O_2 concentrations of 10^{11} molecules per cm^3 in the coated wall flow tube experiments. Because surface coverages of H_2O_2 were low, in the 10^{13} molecules cm^{-2} range, extrapolation to the even lower environmental gas phase and surface concentrations is feasible.[17] H_2O_2 and other polar trace gases adsorption saturate at a so-called monolayer coverage of ~2 to 4×10^{14} molecules cm^{-2}.[16,18] In summary, the increase of H_2O_2 adsorbed to the snow by a factor of 3 when temperatures decrease by 20 K and the fast time response of the adsorbed fraction, as evident in Figure 1, is

https://doi.org/10.1021/acs.est.3c01457
Environ. Sci. Technol. 2023, 57, 11626−11633

consistent with contributing to reported diurnal cycles of H_2O_2 in the polar regions.[6,7] Jacobi et al.[7] described the complex interplay of physical partitioning and snowpack chemistry in polar H_2O_2 observations. This study shows strong partitioning of H_2O_2 to the snowpack at high temperatures where it is subsequently H_2O_2 available for chemistry. The impact of surface adsorption can be expected to decrease with snow age as snow surface area reduces with time during metamorphism.[54] The data in this work now give the basis to address the impact of various snow types and stages of metamorphism.

The uncertainty range of both DIFT data points overlap, indicating that H_2O_2 shows the same equilibrium adsorption behavior as the three types of ice used in this study. Uncertainty might come from the higher gas-phase and resulting surface concentrations of 1.3×10^{14} to 2.6×10^{14} molecules cm^{-2} present during the DIFT experiments (see Supporting Information, "Results, data table"). At these surface coverages approaching a monolayer coverage,[18] adsorbate−adsorbate interactions might start to alter the adsorption process.[17] Additionally, diffusion into the sparse air pores (Figure 1) might contribute to the uncertainty. Nevertheless, this is direct experimental evidence that grain boundaries per se do not play an active role in the surface adsorption of H_2O_2 on short-time scales. Grains are considered large in coated wall ice films resulting in few grain boundaries,[39] which cannot be visualized in these curved and thin samples. We, therefore, refrain from analyzing the diffusive uptake in more detail for these experiments. Comparison of the adsorptive surface coverages with the long-term diffusive uptake for the PC-DIFT (Figure 2B) emphasizes the importance of grain boundaries as a reservoir for the uptake of H_2O_2 from the gas phase in the environment. The diffusive loss term of 7 cm $s^{-1/2}$ for $H\sqrt{D}$ of the PC-DIFT corresponds to a flux of 28×10^{12} molecules per cm^3 and per hour to the snowpack (See Supporting Information "Resistor Model"). For this snowpack, an H_2O_2 adsorption of 2×10^{12} molecules per cm^3 of snow has been estimated above. The flux to the grain boundaries exceeds the number of surface adsorbed molecules by a factor of 10 each hour. Interestingly, in experiments with artificial snow Kerbrat et al.[23] also found a 10 times increase compared to the surface adsorbed HONO each hour at 260 K. Apparently, the slower diffusive HONO loss of 1.6 cm $s^{-1/2}$ for $H\sqrt{D}$ reported by Kerbrat et al.[23] for these snow samples and the lower surface partitioning[23] result in the same relative increase. This back-of-the-envelope comparison illustrates the unmatched strong affinity of H_2O_2 for ice surfaces and the grain boundary network of snow. Similarly, a $H\sqrt{D}$ of 0.02 cm $s^{-1/2}$ for SO_2, a weakly adsorbing trace gas,[19] was found to explain the uptake to artificial snow with negligible surface adsorption. Kinetic modeling results revealed diffusive loss of HNO_3 at 239 K and HCl at 213 K, corresponding to 10 times and 0.7 times the adsorptive surface coverage per hour, respectively.[21,39] Detailed investigation of the relative importance of adsorption and grain boundary diffusion of these species is timely, with focus on the quantification of the grain boundary content in artificial and natural snow and wide variations of temperature and partial pressure. Our results put the relative importance of H_2O_2 diffusive loss on the level with the acidic trace gases, for which the observation of diffusive tailing in uptake curves has kicked off this line of research.[22]

■ ASSOCIATED CONTENT

Supporting Information

The Supporting Information is available free of charge at https://pubs.acs.org/doi/10.1021/acs.est.3c01457.

Sketch of the experimental set-up, description of the data processing, box plot of the recovery results, derivation and results of the resistor model, and table with data (PDF)

■ AUTHOR INFORMATION

Corresponding Author

Thorsten Bartels-Rausch − *Laboratory of Atmospheric Chemistry, Paul Scherrer Institute, Villigen PSI CH-5232, Switzerland;* orcid.org/0000-0002-7548-2572; Email: thorsten.bartels-rausch@psi.ch

Authors

Angela C. Hong − *Department of Chemistry, University of Toronto, Toronto, Ontario M5S 3H6, Canada*

Thomas Ulrich − *Laboratory of Atmospheric Chemistry, Paul Scherrer Institute, Villigen PSI CH-5232, Switzerland*

Erik S. Thomson − *Department of Chemistry and Molecular Biology, Atmospheric Science, University of Gothenburg, Gothenburg SE-41296, Sweden;* orcid.org/0000-0003-2428-7539

Jürg Trachsel − *WSL Institute for Snow and Avalanche Research SLF, Davos Dorf CH-7260, Switzerland*

Fabienne Riche − *WSL Institute for Snow and Avalanche Research SLF, Davos Dorf CH-7260, Switzerland*

Jennifer G. Murphy − *Department of Chemistry, University of Toronto, Toronto, Ontario M5S 3H6, Canada*

D. James Donaldson − *Department of Chemistry, University of Toronto, Toronto, Ontario M5S 3H6, Canada; Department of Physical and Environmental Sciences, University of Toronto Scarborough, Toronto, Ontario M1C 1A4, Canada;* orcid.org/0000-0002-5090-3318

Martin Schneebeli − *WSL Institute for Snow and Avalanche Research SLF, Davos Dorf CH-7260, Switzerland*

Markus Ammann − *Laboratory of Atmospheric Chemistry, Paul Scherrer Institute, Villigen PSI CH-5232, Switzerland;* orcid.org/0000-0001-5922-9000

Complete contact information is available at: https://pubs.acs.org/10.1021/acs.est.3c01457

Notes

The authors declare no competing financial interest.

■ ACKNOWLEDGMENTS

A.H., D.J.D., and J.G.M. thank the Natural Sciences and Engineering Research Council of Canada's CREATE Training Program, the Centre for Global Change Science at the University of Toronto, and the Department of Chemistry at the University of Toronto for funding. T.U., F.R., J.T, M.S., and T.B.R. thank the Swiss National Science Foundation for funding with grants #121857, #140400, and #155999. Initial work, including a guest researcher position for E.S.T., was supported by the European Science Foundation's Micro-Dynamics of ICE (Micro-DICE) research networking program. E.S.T. has also been supported by the Swedish Research Councils, FORMAS (2017-00564), and VR (2020-03497). We thank Mario Birrer for his excellent technical

support and Sepp Schreiber and Sarah Steimer for fruitful discussions.

REFERENCES

(1) Gunz, D. W.; Hoffmann, M. R. Atmospheric chemistry of peroxides: A review. *Atmos. Environ.* **1990**, *24*, 1601−1633.
(2) Anastasio, C.; Robles, T. Light absorption by soluble chemical species in Arctic and Antarctic snow. *J. Geophys. Res.* **2007**, *112*, D24304.
(3) Galbavy, E. S.; Anastasio, C.; Lefer, B. L.; Hall, S. R. Light penetration in the snowpack at Summit, Greenland: Part 1. *Atmos. Environ.* **2007**, *41*, 5077−5090.
(4) France, J. L.; King, M. D.; Lee-Taylor, J. Hydroxyl (OH) radical production rates in snowpacks from photolysis of hydrogen peroxide (H_2O_2) and nitrate (NO_3^-). *Atmos. Environ.* **2007**, *41*, 5502−5509.
(5) Beine, H. J.; Anastasio, C. The photolysis of flash-frozen dilute hydrogen peroxide solutions. *J. Geophys. Res.* **2011**, *116*, D14302.
(6) Jacobi, H.-W.; Bales, R. C.; Honrath, R. E.; Peterson, M. C.; Dibb, J. E.; Swanson, A. L.; Albert, M. R. Reactive trace gases measured in the interstitial air of surface snow at Summit, Greenland. *Atmos. Environ.* **2004**, *38*, 1687−1697.
(7) Jacobi, H.-W.; Frey, M. M.; Hutterli, M. A.; Bales, R. C.; Schrems, O.; Cullen, N. J.; Steffen, K.; Koehler, C. Measurements of hydrogen peroxide and formaldehyde exchange between the atmosphere and surface snow at Summit, Greenland. *Atmos. Environ.* **2002**, *36*, 2619−2628.
(8) Lee, J. K.; Walker, K. L.; Han, H. S.; Kang, J.; Prinz, F. B.; Waymouth, R. M.; Nam, H. G.; Zare, R. N. Spontaneous generation of hydrogen peroxide from aqueous microdroplets. *Proc. Natl. Acad. Sci.* **2019**, *116*, 19294−19298.
(9) Lee, J. K.; Han, H. S.; Chaikasetsin, S.; Marron, D. P.; Waymouth, R. M.; Prinz, F. B.; Zare, R. N. Condensing water vapor to droplets generates hydrogen peroxide. *Proc. Natl. Acad. Sci.* **2020**, *117*, 30934−30941.
(10) Mulvaney, R.; Wolff, E. W.; Oates, K. Sulphuric acid at grain boundaries in Antarctic ice. *Nature* **1988**, *331*, 247−249.
(11) Eichler, J.; Kleitz, I.; Bayer-Giraldi, M.; Jansen, D.; Kipfstuhl, S.; Shigeyama, W.; Weikusat, C.; Weikusat, I. Location and distribution of micro-inclusions in the EDML and NEEM ice cores using optical microscopy and in situ Raman spectroscopy. *Cryosphere* **2017**, *11*, 1075−1090.
(12) Hullar, T.; Anastasio, C. Direct visualization of solute locations in laboratory ice samples. *Cryosphere* **2016**, *10*, 2057−2068.
(13) Morenz, K. J.; Donaldson, D. J. Chemical morphology of frozen mixed nitrate-salt solutions. *J. Phys. Chem. A* **2017**, *121*, 2166−2171.
(14) Bartels-Rausch, T.; Jacobi, H.-W.; Kahan, T. F.; Thomas, J. L.; Thomson, E. S.; Abbatt, J. P. D.; Ammann, M.; Blackford, J. R.; Bluhm, H.; Boxe, C. S.; Dominé, F.; Frey, M. M.; Gladich, I.; Guzman, M. I.; Heger, D.; Huthwelker, T.; Klan, P.; Kuhs, W. F.; Kuo, M. H.; Maus, S.; Moussa, S. G.; McNeill, V. F.; Newberg, J. T.; Pettersson, J. B. C.; Roeselova, M.; Sodeau, J. R. A review of air−ice chemical and physical interactions (AICI): Liquids, quasi-liquids, and solids in snow. *Atmos. Chem. Phys.* **2014**, *14*, 1587−1633.
(15) Ahn, Y. Y.; Kim, J.; Kim, K. Frozen hydrogen peroxide and nitrite solution: The acceleration of benzoic acid oxidation via the decreased pH in ice. *Environ. Sci. Technol.* **2022**, *56*, 2323−2333.
(16) Abbatt, J. P. D. Interactions of atmospheric trace gases with ice surfaces: Adsorption and reaction. *Chem. Rev.* **2003**, *103*, 4783−4800.
(17) Bartels-Rausch, T.; Bergeron, V.; Cartwright, J.; Escribano, R.; Finney, J.; Grothe, H.; Gutiérrez, P.; Haapala, J.; Kuhs, W. F.; Pettersson, J. B. C.; Price, S.; Sainz-Díaz, C.; Stokes, D.; Strazzulla, G.; Thomson, E. S.; Trinks, H.; Uras-Aytemiz, N. Ice structures, patterns, and processes: A view across the icefields. *Rev. Mod. Phys.* **2012**, *84*, 885−944.
(18) Pouvesle, N.; Kippenberger, M.; Schuster, G.; Crowley, J. N. The interaction of H_2O_2 with ice surfaces between 203 and 233 K. *Phys. Chem. Chem. Phys.* **2010**, *12*, 15544−15550.
(19) Clegg, M.; Abbatt, D. Uptake of gas-phase SO_2 and H_2O_2 by ice surfaces: Dependence on partial pressure, temperature, and surface acidity. *J. Phys. Chem. A* **2001**, *105*, 6630−6636.
(20) Ullerstam, M.; Thornberry, T. D.; Abbatt, J. P. D. Uptake of gas-phase nitric acid to ice at low partial pressures: Evidence for unsaturated surface coverage. *Faraday Discuss.* **2005**, *130*, 211−226.
(21) Anthony Cox, R.; Fernandez, M. A.; Symington, A.; Ullerstam, M.; Abbatt, J. P. A kinetic model for uptake of HNO_3 and HCl on ice in a coated wall flow system. *Phys. Chem. Chem. Phys.* **2005**, *7*, 3434−3442.
(22) Abbatt, J. P. D.; Beyer, K. D.; Fucaloro, A. F.; Mcmahon, J. R.; Wooldridge, P. J.; Zhang, R.; Molina, M. J. Interaction of HCl vapor with water-ice - implications for the stratosphere. *J. Geophys. Res.* **1992**, *97*, 15819−15826.
(23) Kerbrat, M.; Huthwelker, T.; Gäggeler, H. W.; Ammann, M. Interaction of nitrous acid with polycrystalline ice: Adsorption on the surface and diffusion into the bulk. *J. Phys. Chem. C* **2010**, *114*, 2208−2219.
(24) Huthwelker, T.; Lamb, D.; Baker, M.; Swanson, B.; Peter, T. Uptake of SO2 by polycrystalline water ice. *J. Colloid Interface Sci.* **2001**, *238*, 147−159.
(25) Huthwelker, T.; Ammann, M.; Peter, T. The uptake of acidic gases on ice. *Chem. Rev.* **2006**, *106*, 1375−1444.
(26) Bartels-Rausch, T.; Wren, S. N.; Schreiber, S.; Riche, F.; Schneebeli, M.; Ammann, M. Diffusion of volatile organics through porous snow: Impact of surface adsorption and grain boundaries. *Atmos. Chem. Phys.* **2013**, *13*, 6727−6739.
(27) Waldner, A.; Artiglia, L.; Kong, X.; Orlando, F.; Huthwelker, T.; Ammann, M.; Bartels-Rausch, T. Pre-melting and the adsorption of formic acid at the air−ice interface at 253 K as seen by NEXAFS and XPS. *Phys. Chem. Chem. Phys.* **2018**, *20*, 24408−24417.
(28) Kong, X.; Waldner, A.; Orlando, F.; Artiglia, L.; Huthwelker, T.; Ammann, M.; Bartels-Rausch, T. Coexistence of physisorbed and solvated HCl at warm ice surfaces. *J. Phys. Chem. Lett.* **2017**, *8*, 4757−4762.
(29) Bartels-Rausch, T.; Orlando, F.; Kong, X.; Artiglia, L.; Ammann, M. Experimental evidence for the formation of solvation shells by soluble species at a nonuniform air-ice interface. *ACS Earth Space Chem.* **2017**, *1*, 572−579.
(30) Krepelova, A.; Bartels-Rausch, T.; Brown, M. A.; Bluhm, H.; Ammann, M. Adsorption of acetic acid on ice studied by ambient-pressure XPS and partial-electron-yield NEXAFS spectroscopy at 230−240 K. *J. Phys. Chem. A* **2013**, *117*, 401−409.
(31) Krepelova, A.; Newberg, J. T.; Huthwelker, T.; Bluhm, H.; Ammann, M. The nature of nitrate at the ice surface studied by XPS and NEXAFS. *Phys. Chem. Chem. Phys.* **2010**, *12*, 8870−8880.
(32) Riche, F.; Schneebeli, M.; Tschanz, S. Design-based stereology to quantify structural properties of artificial and natural snow using thin sections. *Cold Reg. Sci. Technol.* **2012**, *79*−*80*, 67−74.
(33) Riche, F.; Bartels-Rausch, T.; Schreiber, S.; Ammann, M.; Schneebeli, M. Temporal evolution of surface and grain boundary area in artificial ice beads and implications for snow chemistry. *J. Glaciol.* **2012**, *58*, 815−817.
(34) Bartels-Rausch, T.; Guimbaud, C.; Gäggeler, H. W.; Ammann, M. The partitioning of acetone to different types of ice and snow between 198 and 223 K. *Geophys. Res. Lett.* **2004**, *31*, L16110.
(35) Thomson, E. S.; Wettlaufer, J. S.; Wilen, L. A. A direct optical method for the study of grain boundary melting. *Rev. Sci. Instrum.* **2009**, *80*, 103903.
(36) Granger, R.; Flin, F.; Ludwig, W.; Hammad, I.; Geindreau, C. Orientation selective grain sublimation−deposition in snow under temperature gradient metamorphism observed with diffraction contrast tomography. *Cryosphere* **2021**, *15*, 4381−4398.
(37) Roscoat, S. R. d.; King, A.; Philip, A.; Reischig, P.; Ludwig, W.; Flin, F.; Meyssonnier, J. Analysis of snow microstructure by means of X-ray diffraction contrast tomography. *Adv. Eng. Mater.* **2011**, *13*, 128−135.

https://doi.org/10.1021/acs.est.3c01457
Environ. Sci. Technol. 2023, 57, 11626−11633

(38) Conklin, M. H.; Sigg, A.; Neftel, A.; Bales, R. C. Atmosphere-snow transfer-function for H_2O_2 - microphysical considerations. *J. Geophys. Res.* **1993**, *98*, 18367−18376.
(39) McNeill, V. F.; Geiger, F. M.; Loerting, T.; Trout, B. L.; Molina, L. T.; Molina, M. J. Interaction of hydrogen chloride with ice surfaces: The effects of grain size, surface roughness, and surface disorder. *J. Phys. Chem. A* **2007**, *111*, 6274−6284.
(40) Davidovits, P.; Kolb, C. E.; Williams, L. R.; Worsnop, D. R.; Jayne, J. T.; Worsnop, D. R.Update 1 of: Mass Accommodation and Chemical Reactions at Gas−Liquid Interfaces, *Chem. Rev.* **2011**, *111*, DOI: 10.1021/cr100360b
(41) Ammann, M.; Pöschl, U. Kinetic model framework for aerosol and cloud surface chemistry and gas-particle interactions - part 2: Exemplary practical applications and numerical simulations. *Atmos. Chem. Phys.* **2007**, *7*, 6025−6045.
(42) Pöschl, U.; Rudich, Y.; Ammann, M. Kinetic model framework for aerosol and cloud surface chemistry and gas-particle interactions - part 1: General equations, parameters, and terminology. *Atmos. Chem. Phys.* **2007**, *7*, 5989−6023.
(43) Sander, R. Compilation of Henry's law constants (version 4.0) for water as solvent. *Atmos. Chem. Phys.* **2015**, *15*, 4399−4981.
(44) Thibert, E.; Dominé, F. Thermodynamics and kinetics of the solid solution of HCl in ice. *J. Phys. Chem. B* **1997**, *101*, 3554−3565.
(45) Thibert, E.; Dominé, F. Thermodynamics and kinetics of the solid solution of HNO_3 in ice. *J. Phys. Chem. B* **1998**, *102*, 4432−4439.
(46) Morenz Korol, K. J.; Kumayon, I. M.; Kahan, T. F.; Donaldson, D. J. Chemical morphology controls reactivity of OH radicals at the air-ice interface. *J. Phys. Chem. A* **2021**, *125*, 8925−8932.
(47) Baker, I. Microstructural characterization of snow, firn and ice. *Philos. Trans. R. Soc., A* **2019**, *377*, 20180162.
(48) Pinzer, B. R.; Schneebeli, M. Snow metamorphism under alternating temperature gradients: Morphology and recrystallization in surface snow. *Geophys. Res. Lett.* **2009**, *36*, L23503.
(49) Crowley, J. N.; Ammann, M.; Cox, R. A.; Hynes, R. G.; Jenkin, M. E.; Mellouki, A.; Rossi, M. J.; Troe, J.; Wallington, T. J. Evaluated kinetic and photochemical data for atmospheric chemistry: Volume V − heterogeneous reactions on solid substrates. *Atmos. Chem. Phys.* **2010**, *10*, 9059−9223.
(50) Zimmermann, S.; Kippenberger, M.; Schuster, G.; Crowley, J. N. Adsorption isotherms for hydrogen chloride (HCl) on ice surfaces between 190 and 220 K. *Phys. Chem. Chem. Phys.* **2016**, *18*, 13799−13810.
(51) Dominé, F.; Cabanes, A.; Taillandier, A.-S.; Legagneux, L. Specific surface area of snow samples determined by CH_4 adsorption at 77 K and estimated by optical microscopy and scanning electron microscopy. *Environ. Sci. Technol.* **2001**, *35*, 771−780.
(52) Kerbrat, M.; Pinzer, B.; Huthwelker, T.; Gäggeler, H. W.; Ammann, M.; Schneebeli, M. Measuring the specific surface area of snow with X-ray tomography and gas adsorption: Comparison and implications for surface smoothness. *Atmos. Chem. Phys.* **2008**, *8*, 1261−1275.
(53) Hutterli, M. A.; McConnell, J. R.; Chen, G.; Bales, R. C.; Davis, D. D.; Lenschow, D. H. Formaldehyde and hydrogen peroxide in air, snow and interstitial air at South Pole. *Atmos. Environ.* **2004**, *38*, 5439−5450.
(54) Legagneux, L.; Cabanes, A.; Dominé, F. Measurement of the specific surface area of 176 snow samples using methane adsorption at 77 K. *J. Geophys. Res.* **2002**, *107*, ACH 5-1−ACH 5-15.

https://doi.org/10.1021/acs.est.3c01457
Environ. Sci. Technol. 2023, 57, 11626−11633